



## Two-Dimensional vs. Three-Dimensional Clustering and Percolation in Fields of Overlapping Ellipsoids

Y.-B. Yi,<sup>a</sup> C.-W. Wang,<sup>a</sup> and A. M. Sastry<sup>a,b,\*</sup>

<sup>a</sup>Department of Mechanical Engineering and <sup>b</sup>Department of Biomedical Engineering, University of Michigan, Ann Arbor, Michigan 48109-2125, USA

Maximum depth-to-particle-dimension ratios in which systems can be treated as two-dimensional (2D) rather than three-dimensional (3D) systems in determining percolative properties have not been reported. This problem is of great technological significance. 3D solutions for percolation in even low-density systems pose much more intensive computational problems than their 2D analogs and also result in significantly different predictions for percolation onset. Moreover, many materials and sensing applications require analysis of domains of finite thickness. Adequate loading of particles is required, *e.g.*, in electrodes in advanced batteries and fuel cells to ensure good conductivity. Adequate deployment of sensors into fields of finite thickness such as oblate, neuronal cells is required, *e.g.*, to detect specific ions. A systematic determination of the effect of these arrangements on percolation properties is needed for both applications. Here, we provide comparisons of cluster sizes, densities, and percolation points among monodisperse, 2D and 3D systems of overlapping ellipsoids by systematically increasing the depth of the 3D system relative to particle dimensions. We investigate the effect of several boundary condition assumptions on the resulting particle orientations, emphasizing the probability of formation of large clusters. A method of experimental determination of percolation onset is also suggested, using the maximum change in cluster size.

© 2004 The Electrochemical Society. [DOI: 10.1149/1.1769272] All rights reserved.

Manuscript received November 7, 2003. Available electronically July 20, 2004.

Producing conductive, thinly layered structures for use as battery electrodes requires some estimation of the amount, shape, and distribution of conductive additive, *e.g.*, conductive carbons in Li-ion batteries.<sup>1,2</sup> Determining the dimensionality of these systems for purposes of modeling percolative properties is critical, because two-dimensional (2D) and three-dimensional (3D) percolation points depend upon both particle shape and system thickness. However, maximum depth-to-particle-dimension ratios in which systems can be treated as 2D rather than 3D systems for purposes of modeling percolation have not yet been reported quantitatively.

Accurate and efficient simulation of percolation in overlapping fields is also important in the design of sensor systems,<sup>3-5</sup> material properties in materials containing interpenetrating particles,<sup>6-9</sup> and even epidemiology.<sup>10-13</sup> Some of these problems are inherently 2D, as in epidemiology, wherein the overlapping “particles” represent scalar fields of magnitudes of disease transmissibility around any single source. In almost all materials applications, and in sensor design for detection of species or phenomena, domains are often fully 3D and represent physical space. For example, in nanostructured gas sensors, the presence of a gas increases the conductivity of the sensing material at the grain boundaries in 3D.<sup>14,15</sup> Importantly, percolation points in 2D vs. 3D model domains have been shown to be different, analytically,<sup>16-19</sup> numerically,<sup>20-24</sup> and experimentally,<sup>25</sup> and thus determination of the appropriate dimensionality of a model system is critical. Many materials applications of percolation modeling require analysis of “thin” sections, *e.g.*, layered electrodes in advanced batteries or fuel cells.<sup>26,27</sup> Sensing applications for finite, oblate domains are also abundant, *e.g.*, intracellular sensing.<sup>28-30</sup> Thus, we hereafter use the terms “field” and “particle” interchangeably, and note that our interests center on percolation in fields of fully permeable particles, an unrealistic condition for high-density material additives, but quite satisfactory for low-density arrangements of additives and for all sensing applications.

Three general approaches have been historically used to determine percolation onset in particle systems. One approach is to analytically approximate percolation onset, via a power series expansion of mean cluster density. In a series of the authors’ recent papers on percolation phenomena, *e.g.*, Ref. 31, approximate analytical methods were developed to determine the percolation threshold for systems of ellipses and ellipsoids, building on classic work in the percolation of systems of spheres and circles.<sup>16,18,32</sup> Mean cluster

size, defined as the average number of particles in clusters in a fixed domain, was used in this work. Specifically, the mean cluster size was expressed in the form of a power series, allowing the development of a convergence criterion for percolation based upon particle density, following Coniglio’s formulation.<sup>33,34</sup> Though the analytical methods developed were accurate, they were also computationally intensive due to the required evaluation of integrals, especially when high-order connecting graphs were introduced.

A second approach is to conduct large-scale Monte Carlo simulations (being careful to select domains large enough to avoid scale dependencies in solutions) for particular geometries of particles and domains;<sup>24,35</sup> this approach is also commonly used to validate analytical approximations.<sup>19,31</sup> A third approach is to use either approximations or direct simulations to develop semiempirical guidelines for percolative properties (based, for example, on geometry, cluster statistics, or domain size).

However, most percolation and aggregate models have been developed for infinite systems, either in unbounded systems, or in pseudoinfinite systems with periodic boundaries, though the importance of boundary effects has been noted by a number of groups.<sup>36-39</sup> For example, Gabrielli *et al.*<sup>40</sup> studied the effect of boundaries on geometrical properties and found that the fractal dimension of the percolating cluster near the boundary was remarkably different from the bulk one. Thomsen<sup>41</sup> investigated the critical correlation length exponents and percolation thresholds in quasi-2D site percolation systems, with finite interplane coupling. He found the percolation threshold to vary continuously from 2D to 3D values with a power-law exponential relationship. Examples of work in specialized domains include that of Lorenz and Ziff,<sup>42</sup> who studied percolation and clustering on spherical surfaces; Tsubakihara,<sup>43</sup> who examined site percolation in a rectangular system of aspect ratio greater than one; and Provatas *et al.*,<sup>44</sup> who investigated 2D fiber networks generated via a simulated flocculation process, resulting in localized particle agglomeration. Several studies have also been published on specific finite size effects and scaling approaches for 2D systems (*e.g.*, Ref. 45-47), but the dimensional crossover in cluster properties and percolation thresholds has not been determined for continuum systems, to the authors’ knowledge.

With the improved computational capabilities attained over the past few years, it is now possible to simulate a domain nearly the size of the physical domain of interest in many applications, especially in sensing nanotechnologies for biological materials, *e.g.*, intracellular sensing.<sup>48,29</sup> Models of permeable fields of geometrically complex shapes are critically important in such applications, because many targeted nanoprobe (including molecule uses in free

\* Electrochemical Society Active Member.

<sup>z</sup> E-mail: amsastry@umich.edu

dyes) have an inherent directionality,<sup>49</sup> *i.e.*, they contain specific endgroups which comprise the detector, which renders the shape of the detection field nonspheroidal, but perhaps ellipsoidal. Thus, in the present work, we compare our prior analytic approximations to percolation onset in 2D and 3D continua with Monte Carlo simulations, designed to provide comparisons of

1. cluster properties and percolation behavior between 2D and 3D continuum systems containing equisized, overlapping ellipsoids, by systematically increasing the depth of a 3D system of particles and determining percolation points and cluster sizes and densities; and

2. the effects of varying boundary conditions in particle orientation within the systems, accounting for constraints imposed by boundaries on the formation of large clusters.

We also suggest some important considerations in image analysis of porous materials using these results, including interpretation of cluster formation as either random or physically based and determination of the effect of processes such as pressing on cluster densities by comparison with random cluster formations expected in finite systems.

### Detection of Particle Overlap

The detection of particle overlap comprises a very computationally intensive step in both analytical approximations and Monte Carlo simulations of percolation onset in systems of permeable, ellipsoidal particles. In principle, one can solve the governing equations of ellipsoidal surfaces and determine whether real solutions exist. But the computational effort in doing so is high; therefore, some workers have developed indirect, but computationally efficient criteria.

To describe these criteria, the concept of a “contact function” must be introduced. Suppose the contact function  $F$  for a single ellipsoid  $A$ , specified by the location  $r_A$  of its center, and the angle  $\Omega_A$ , which expresses its orientation in space, can be written as  $F_A(r - r_A, \Omega_A)$ . We then have  $F < 1$ , for  $r$  inside  $A$ ;  $F = 1$  for  $r$  located on the surface of  $A$ ; and  $F > 1$  for  $r$  outside  $A$ . A nonunique but obvious choice for  $F$  is

$$F_A(r - r_A, \Omega_A) = (r - r_A)^T A^{-1} (r - r_A) \quad [1]$$

where  $T$  indicates the transpose, and

$$A(\Omega_A) = \sum_{i=1}^3 R_i(\Omega_A) R_i^T(\Omega_A) \quad [2]$$

where  $R$  are the vectors comprising the semiaxes.

For two ellipsoids of arbitrary shape and size, Perram and Wertheim<sup>50</sup> proved rigorously that the function  $G(r, l)$ , defined as

$$G(r, \lambda) = \lambda F_A(r) + (1 - \lambda) F_B(r) \quad [3]$$

has a minimum

$$G_{\min} = \lambda(1 - \lambda) r_{AB}^T [\lambda B + (1 - \lambda) A]^{-1} r_{AB} \quad [4]$$

They further showed that

$$H = \max(G_{\min}) \quad [5]$$

is the contact function for two ellipsoids; namely, for  $H < 1$ , the two ellipsoids overlap, for  $H = 1$  they are tangent, and for  $H > 1$  they are separate. We note that this contact function is implicit, and thus its evaluation requires numerical iteration. For ellipsoids of uniform size, Viellard-Baron<sup>51</sup> derived a more efficient, explicit expression for overlap detection. A necessary and sufficient condition was stated for two ellipsoids to have no real point in common, or to be exteriorly tangential, using a contact function involving several variables for the geometry and relative spatial locations of the ellipsoids. Because we are presently interested in the

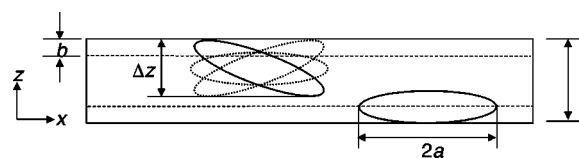


**Figure 1.** Schematic of the finite thickness model with extreme positions/orientations of ellipsoidal particles shown.

effects of dimension, rather than particle size distribution, we implement the condition stated by Viellard-Baron, for equisized particles. We point out that Garboczi *et al.*<sup>24</sup> also used Baron’s overlap criterion. However, they dealt with the infinite 3D problem, whereas we have worked in finite systems. The technique can easily be extended to the problem involving ellipsoids of variable sizes by replacing Viellard-Baron’s overlap criteria with Perram’s contact function.

### Monte Carlo Simulations

We simulated domains comprised of spatially uncorrelated, equisized ellipsoids in a 3D ( $L \times L \times D$ ) continuum. For simplicity, the centers of the ellipsoids were distributed by a Poisson process. In a real material, particle density near a surface may be somewhat higher than in the center, *e.g.*, for packing or stamping postprocesses for shaping of porous materials, though this was neglected here for simplicity. And, although particle geometry and size frequently vary in real materials, prior studies have shown that a mild variation in particle size does not change the clustering properties substantially.<sup>52</sup> In all simulations, periodic boundary conditions were applied to the edges of the  $x$ - $y$  plane, to minimize boundary effects. No periodicity was imposed in the  $z$  direction.

Particle orientation angles were randomly distributed, with extreme inclinations determined for a particular, semi-infinite domain as follows. By introduction of a frame of reference wherein  $x$  and  $y$  represented the infinite dimensions, and  $z$  represented the finite dimension, particles were assumed to be oriented with a uniform distribution function  $[0, 2\pi]$  in the  $x$ - $y$  plane (and we note that the distribution function may also be written for  $[0, \pi]$  if symmetry about either the  $x$  or  $y$  axis is considered). The difference of the two extreme locations on the ellipsoidal surface in the  $z$  direction  $\Delta z$ , is the maximum possible difference of the extreme locations on the ellipsoidal surface at the given location  $z$  of the particle centerpoint; as shown in Fig. 1. It can be expressed as

$$\Delta z = 2\sqrt{b^2 \sin^2 \theta + a^2 \cos^2 \theta} \quad [6]$$

The distribution function of the elevation angle of the major axis of particle over the  $z$  direction can be derived from this expression, as

$$\Theta = \cos^{-1} \left( \sqrt{\frac{(\Delta z/2)^2 - b^2}{a^2 - b^2}} \right) (1 - 2\Theta^*) \quad [7]$$

where  $\Theta^*$  is a random number distributed in  $[0, 1]$ . Thus, we have, for the half-height

$$\Delta z/2 = \min\{a, z, c - z\} \quad [8]$$

We note that one limiting case of elevation orientation angle distribution is simply uniform particle alignment with respect to the  $x$ - $y$  plane. We denote this case the “parallel model” and analyze it specifically because it has some importance in the manufacture of certain materials, *e.g.*, laminated materials, wherein alignment is induced. This constraint on particle orientation results in an overall reduction of interparticle connections and therefore a higher percolation threshold relative to the random case.

### Percolation Threshold Detection

Percolation onset for 2D and 3D continua was studied by systematically increasing the  $z$  dimension (thickness) of model domains

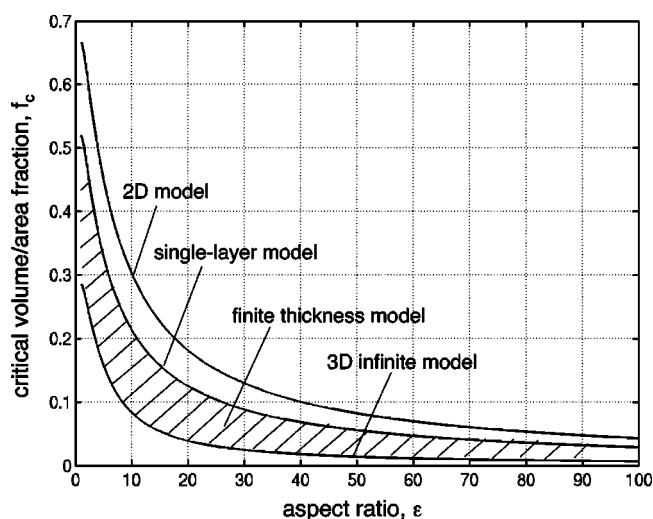


**Figure 2.** Comparison of percolation thresholds in 2D, 3D, and single-layer model simulations.

and recording the percolation threshold at which a cluster connecting the two  $x$ - $z$  boundary faces is detected, where  $z$  is the dimension having finite thickness. Percolation volume fractions vs. aspect ratios are shown for four types of domains in Fig. 2: (i) a 2D arrangement, wherein ellipses were generated in a 2D domain (from results reported in Ref. 19); (ii) a “single-layer” arrangement of ellipses, wherein a normalized thickness of  $t/b = 1$  was used,  $t$  is the half-layer thickness; (iii) a “finite thickness” model, wherein the  $z$  dimension was specified relative to the particle size; and (iv) a 3D (infinite) model (from results reported in Ref. 53). We note that the single-layer domain, comprised of a single layer of particles with major axes parallel to the  $x$ - $y$  plane, is merely a degenerate case of the finite-layer domain. Interparticle overlap in this case is determined by the elliptical geometry of the midplane ( $x$ - $y$ ) cross section. Comparison of the volume of the ellipsoid  $(3/4)\pi ab^2$  and the area  $\pi ab$  of the ellipse allows derivation of a relationship for the critical volume fraction  $f_c$  of the single-layer model in terms of the critical area fraction  $f_a$  in the 2D problem, as

$$f_c = 1 - (1 - f_a)^{2/3} \quad [9]$$

using the following relation for particle density  $\rho$ , and area or volume of a single particle  $\sigma$

$$f = 1 - e^{-\rho\sigma} \quad [10]$$

The results in Fig. 2 for the 2D and 3D infinite models were obtained by averaging the results of 1000 simulations, each consisting of at least 5000 particles. Results for the single-layer model were

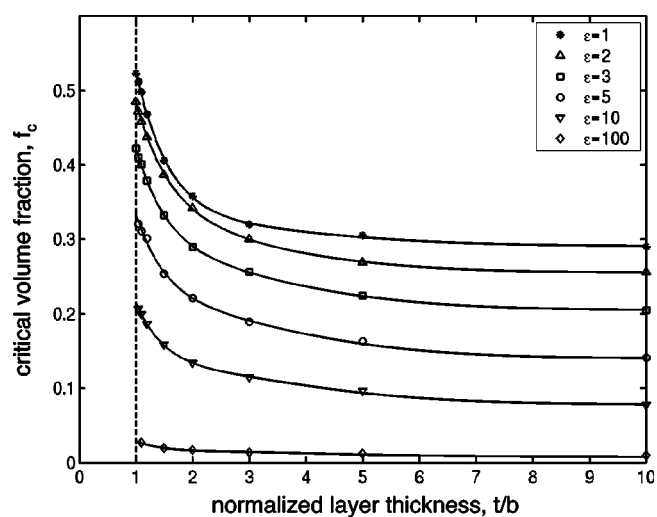


**Figure 3.** Critical volume fraction  $f_c$  for the finite thickness model as a function of the normalized layer thickness  $t/b$ . Approximately 10,000 particles were generated in each case for determination of percolation thresholds.

based on the corresponding 2D model and obtained via Eq. 9. Values for other geometries can be readily interpolated from these computational results.

These results and approximate relations clearly demonstrate the importance of dimensionality in real domains in the prediction of percolation onset, particularly for higher aspect ratio particles. And, the intrinsic variability of percolation onset in finite-thickness systems is high: even for the sphere problem, the percolation threshold rises from 29 to 52.3%, with a ratio of domain edge lengths of 1:1.80. For higher aspect ratios, the relative variability can be even higher. For example, for particles of  $\epsilon = 10$ , the percolation threshold is between  $\sim 6.8$  and  $\sim 21.2\%$ , with an edge ratio of 1:3.11. Thus, clearly, the 2D or 3D models are only applicable when the thickness is either very small or extremely large, respectively, relative to particle dimension.

In Fig. 3, critical volume fractions  $f_c$  are reported for the finite-thickness domains, as a function of layer thickness  $t$ ; results for  $1 \leq \epsilon \leq 100$  are shown. For convenient reference, we have included our own compilation of critical volume fractions using an approximate formula which shows excellent agreement with our numerical results<sup>19,53</sup> in Table I; each fitted curve gave a correlation factor with numerical results  $\geq 0.99$ . In Fig. 3, cell thicknesses are normalized by the half-length of particle minor axis  $b$ , so that the points on the left of each curve represent single-layer configurations, and solutions asymptotically approach those for the infinite 3D model as  $t \rightarrow \infty$ . As with the infinite domains, the percolation threshold drops rapidly with an increase in the particle aspect ratio  $\epsilon$ .

**Table I.** Critical volume fraction  $f_c$  as function of normalized layer thickness  $z = t/b$  ( $t$  is half-layer thickness;  $b$  is half-length of particle minor axis), based on approximate formula  $f_c = C_1 + (C_2 + C_3z + C_4z^2)e^{-z}$ .

$\epsilon$	$C_1$	$C_2$	$C_3$	$C_4$	$R^a$	$f_c(z=1)^b$	$f_c(z=\infty)^b$
1	0.2908	1.0899	-0.5941	0.1458	0.9997	0.531	0.290
2	0.2550	0.8727	-0.3767	0.1290	0.9999	0.488	0.252
3	0.2047	0.8958	-0.4726	0.1715	0.9999	0.418	0.203
5	0.1397	0.8139	-0.4623	0.1776	0.9992	0.333	0.137
10	0.0779	0.6299	-0.4062	0.1493	0.9997	0.212	0.0724
100	0.0076	0.1195	-0.0935	0.0326	0.9905	0.028	0.0052

<sup>a</sup>  $R$  is the correlation factor for each curve.

<sup>b</sup> Values of  $f_c$  for the limiting configurations 2D ( $z = 1$ ) and 3D ( $z = \infty$ ).

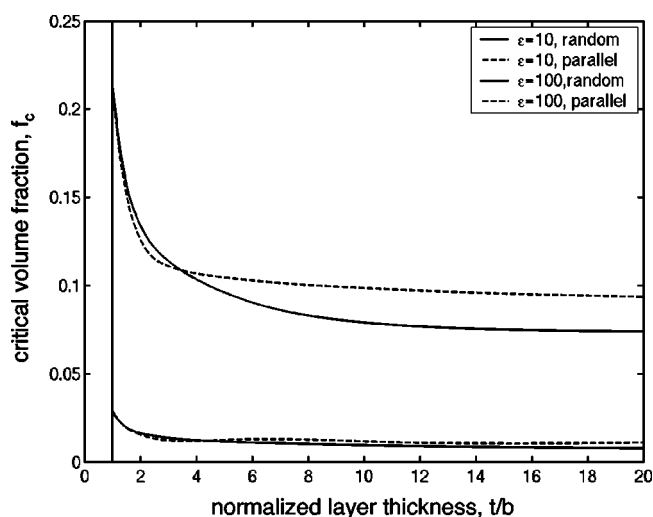


**Figure 4.** Comparison of the critical volume fractions for the parallel and random models, vs. normalized layer thickness  $t/b$ . Approximately 10,000 particles were generated in each case for determination of percolation thresholds.

For example, the critical volume fraction of  $\epsilon = 1$  is more than 50 times that of  $\epsilon = 100$  at large thickness.

Further, the percolation threshold dropped quickly, initially, with increasing thickness, but reached a plateau for all aspect ratios studied, when  $t$  exceeds 10. Roughly speaking, in the range of  $\epsilon = 1-100$ , our results show that the infinite model can be used to accurately approximate the percolation threshold for domain thicknesses  $\sim 5$  times greater than particle thickness  $2b$ . Otherwise, a finite-thickness model must be used to incorporate the effects of the boundary, for accurate prediction of percolation onset. This result has important implications for modeling of many engineered “thin films” or other layered materials (e.g., Ref. 54 and 55), in which the layer thickness is frequently more than an order of magnitude larger than the particle thickness: an infinite 3D model is more suitable for these materials than a 2D model.

Figure 4 shows a comparison of critical volume fraction for the parallel and random models as a function of layer thickness. The percolation threshold for the parallel model is significantly higher

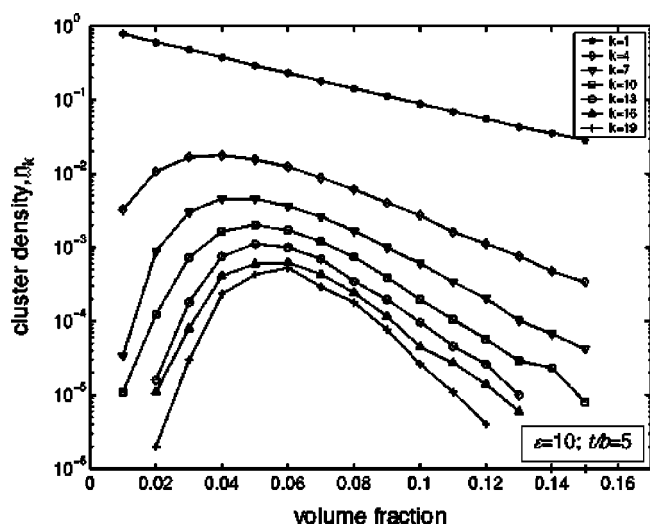
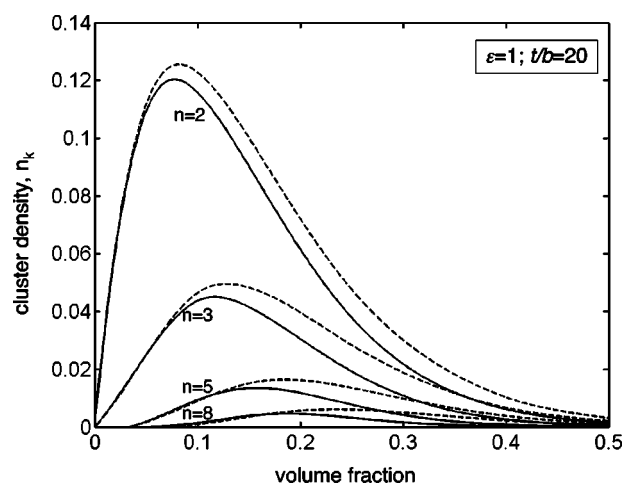
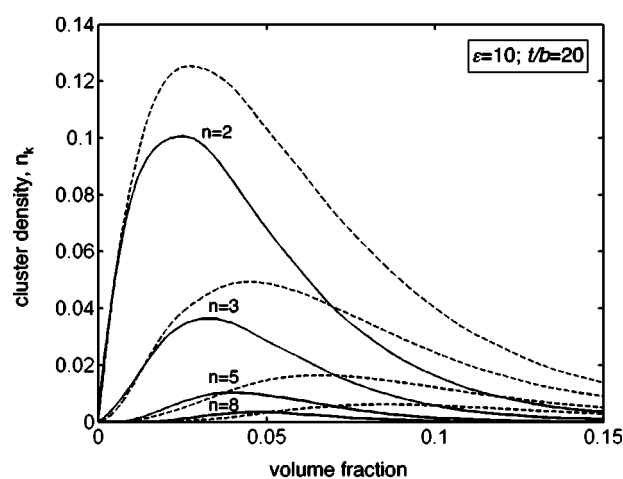


**Figure 5.** Cluster density vs. volume fraction for ellipsoids of aspect ratio 10,  $t/b = 5$ . Approximately 10,000 particles were involved in each realization.



(a)



(b)

**Figure 6.** Cluster densities ( $n = 2, 3, 5, 8$ ) from simulations (solid lines) vs. Roach's approximations (Eq. 11, dashed lines), for (top) spheres ( $f_c = 0.29$ ) and (bottom) ellipsoids of aspect ratio 10 ( $f_c = 0.072$ ). Fully 3D models (unit window dimensions with  $\sim 10,000$  particles in each case) were used in the simulations.

than for the random model, once the thickness exceeds a few times the particle thickness. This is undoubtedly due to the reduction in overall likelihood of interparticle connections in the  $z$  direction for the parallel model. Any constraint applied to the orientations or locations of particles generally reduces interparticle connectivity and increases the percolation threshold. This effect is more pronounced for thin layers, though in the limiting case of thickness reduction to a single layer, the solutions coincide, as seen by the rapid convergence of the two solutions around  $t/b = 2$  in Fig. 4.

### Cluster Property Determination

The generation of statistical distributions of large clusters has proven computationally and analytically daunting: for example, there are 528 possible ways to form a cluster of only five particles,<sup>19,53</sup> making it practically impossible to assemble statistics for the systems of 10,000-100,000 particles, using older computer processors. More effort has been spent in generating data on small-cluster statistics, wherein isolated clusters containing a fixed, small number of particles were sought using connecting graphs, namely, schematics reflecting the pairwise connectivity between particles in-

**Table II. Percentage of ellipsoidal particles belonging to clusters of size  $k$  under different volume fraction  $f$  for 2D configurations.**

$f$	$\epsilon = 1$							$\epsilon = 10$						
	0.5%	1.0%	2.0%	5.0%	10%	20%	30%	0.5%	1.0%	2.0%	5.0%	10%	20%	30%
$k = 1$	0.973	0.945	0.893	0.741	0.529	0.259	0.119	0.928	0.853	0.739	0.442	0.199	0.035	0.006
$k = 2$	0.027	0.051	0.092	0.195	0.262	0.203	0.109	0.069	0.124	0.186	0.240	0.136	0.017	0.002
$k = 3$	*	0.004	0.012	0.046	0.119	0.152	0.096	0.003	0.017	0.060	0.129	0.108	0.013	0.001
$k = 4$	*	*	0.002	0.014	0.052	0.117	0.085	*	0.006	0.012	0.079	0.091	0.011	0.001
$k = 5$	*	*	0.001	0.003	0.022	0.079	0.071	*	*	0.003	0.041	0.072	0.013	*
$k = 6$	*	*	*	*	0.010	0.063	0.059	*	*	*	0.033	0.061	0.009	*
$k = 7$	*	*	*	*	0.003	0.035	0.061	*	*	*	0.010	0.046	0.009	*
$k = 8$	*	*	*	*	0.001	0.037	0.041	*	*	*	0.011	0.037	0.009	*
$k = 9$	*	*	*	*	*	0.017	0.048	*	*	*	0.007	0.029	0.008	*
$k = 10$	*	*	*	*	*	0.016	0.036	*	*	*	0.003	0.032	0.008	*
$k = 20$	*	*	*	*	*	*	0.016	*	*	*	*	0.006	0.012	*

Asterisks (\*) are used for percentages less than 0.1% (*i.e.*, fractions smaller than 0.001). The 2D volume fraction is related to area fraction via Eq. 9. Results are averaged from 10 realizations, each involving approximately 10,000 particles.

side each cluster.<sup>17,18</sup> This method does not require full knowledge of the connectivity of the structure and is thus extremely efficient for examination of clusters of four or fewer particles.

As a useful approximation, Roach<sup>56</sup> suggested that at low volume fraction for particles of any shape, the cluster density  $n_k$  could be estimated from

$$n_k \approx \frac{n_1(1 - n_1)^{k-1}}{k} \quad [11]$$

Ogston and Winzor<sup>57</sup> provided an analytical expression for the excluded volume of an ellipsoid, which can be used to derive the exact solution of  $n_1$  for ellipsoids, as follows

$$n_1 = \exp \left\{ -\frac{4}{3} \pi a b^2 \rho \left( 2 + \left\{ \frac{3}{2} + \frac{3}{4} \frac{(2\epsilon^2 - 1)}{\epsilon^4 - \epsilon^2} \ln(2\epsilon^2 - 1) \right\} \right) \right. \\ \left. \times \left\{ \frac{\sqrt{2\epsilon^2 - 1}}{\epsilon} + \frac{\epsilon^3 \sin^{-1} \left( \frac{\epsilon^2 - 1}{\epsilon^2} \right)}{\epsilon^2 - 1} \right\} \right\} \quad [12]$$

For spheres, *i.e.*,  $\epsilon = 1$ ,  $n_1$  becomes

$$n_1 = \exp \left( -\frac{32}{3} \pi r^3 \rho \right) \quad [13]$$

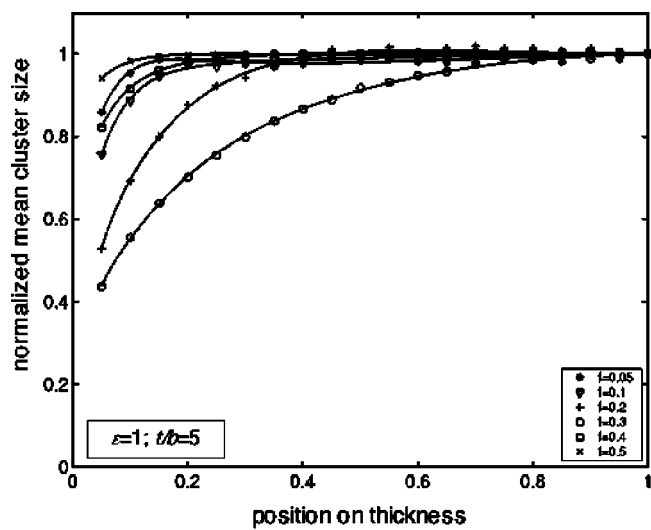
To analyze large clusters, we developed an alternative simulation approach. Briefly, we first assumed that each particle formed a distinct cluster. Clusters with at least one pair-connection were identified by checking interparticle connectivity, and subsequently merged. This process was repeated  $(n - 1)(n - 2)/2$  times, for  $n$  particles. Using this approach, the interconnectivity of each and every pair of particles was examined and catalogued, and thus the complete network structure was obtained. By tallying the number of clusters with  $k$  particles, and averaging the results over a number of realizations, we obtained mean densities of clusters, for higher values of  $k$  ( $k > 4$ ) than reported previously.

We thus numerically determined, for lower volume fractions of ellipsoids, both cluster densities (Fig. 5), and mean cluster sizes in the  $z$  direction (Fig. 7). As shown in Fig. 5 (for ellipsoids of aspect ratio 10,  $t/b = 5$ ), for low volume fractions, clusters comprised of isolated particles dominate, and mean cluster sizes are therefore close to unity. At higher volume fractions, isolated particles become rarer, consistent with our previous computational results for both 2D and 3D networks.<sup>19,53</sup> Roach's approximations are plotted along with numerical results for several values on Fig. 6, showing generally good agreement for volume fractions less than half of the percolation threshold, but significant divergence from actual values beyond the critical volume fraction. Table II reports the fractions of cluster sizes present, for 2D systems, and Table III reports them for 3D systems. Interestingly, even at volume fractions as low as 2%, a

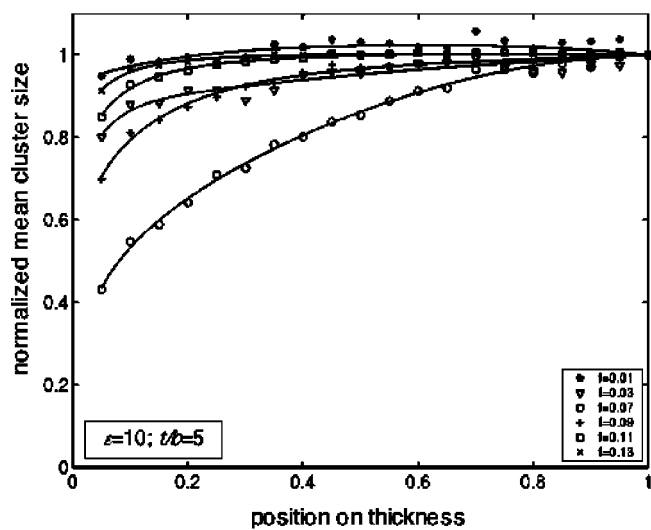
**Table III. Percentage of ellipsoidal particles belonging to clusters of size  $k$  under different volume fraction  $f$  for 3D configurations.**

$f$	$\epsilon = 1$							$\epsilon = 10$						
	0.5%	1.0%	2.0%	5.0%	10%	20%	30%	0.5%	1.0%	2.0%	5.0%	10%	20%	30%
$k = 1$	0.959	0.922	0.851	0.665	0.431	0.180	0.061	0.871	0.800	0.615	0.279	0.074	0.007	0.001
$k = 2$	0.038	0.070	0.122	0.218	0.232	0.125	0.042	0.113	0.147	0.208	0.135	0.025	0.001	*
$k = 3$	0.003	0.008	0.023	0.074	0.132	0.083	0.031	0.016	0.038	0.079	0.090	0.014	*	*
$k = 4$	*	*	0.003	0.028	0.077	0.075	0.025	*	0.006	0.041	0.069	0.009	*	*
$k = 5$	*	*	*	0.009	0.047	0.064	0.016	*	0.003	0.023	0.049	0.008	*	*
$k = 6$	*	*	*	0.003	0.030	0.047	0.013	*	0.003	0.011	0.036	0.003	*	*
$k = 7$	*	*	*	0.001	0.018	0.045	0.016	*	*	0.005	0.029	0.003	*	*
$k = 8$	*	*	*	0.001	0.012	0.032	0.015	*	*	0.002	0.027	0.001	*	*
$k = 9$	*	*	*	*	0.006	0.033	0.009	*	*	0.005	0.020	0.001	*	*
$k = 10$	*	*	*	*	0.004	0.025	0.010	*	*	0.003	0.027	*	*	*
$k = 20$	*	*	*	*	*	0.011	0.008	*	*	*	0.010	0.001	*	*

Asterisks (\*) are used for percentages less than 0.1% (*i.e.*, fractions smaller than 0.001). Results are averaged from 10 realizations, each involving approximately 10,000 particles.

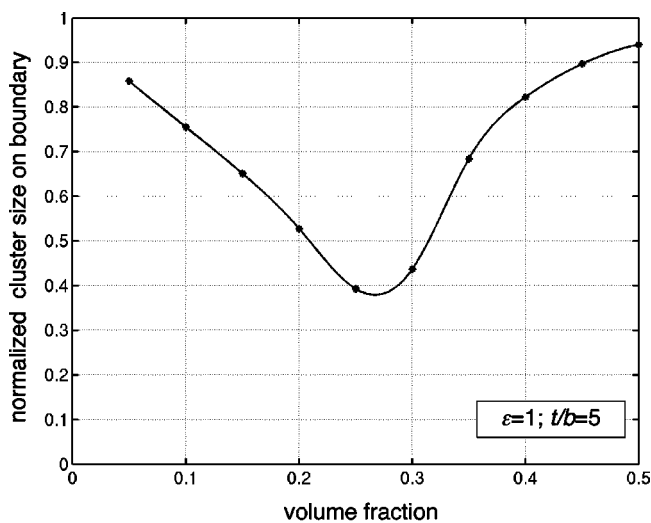


(a)

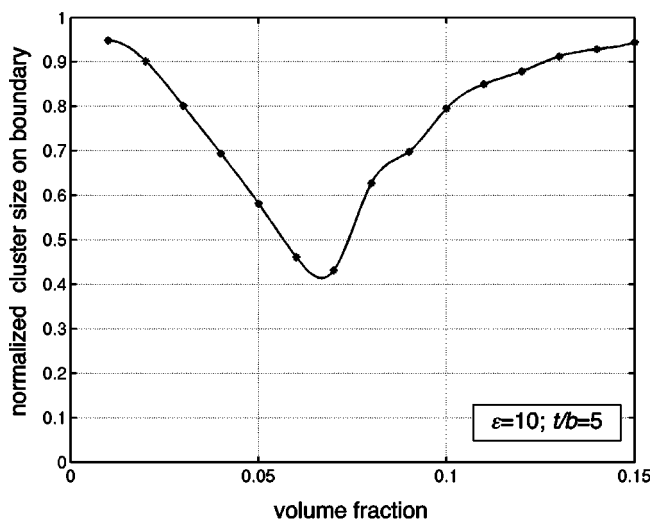


(b)

**Figure 7.** Mean cluster sizes vs.  $z$  location (*i.e.*, normalized position in the thickness, where 0 and 1 are the lower and middle surfaces, respectively) in systems of (top) spheres and (bottom) ellipsoids ( $\epsilon = 10$ ) for various volume fractions at  $t/b = 5$ . 10,000 particles were used in each simulation.



(a)



(b)

**Figure 8.** Normalized mean cluster sizes vs. volume fraction in systems of (top) spheres and (bottom) ellipsoids ( $\epsilon = 10$ ), at the boundary. Ten thousand particles were used in each simulation;  $t/b = 5$ .

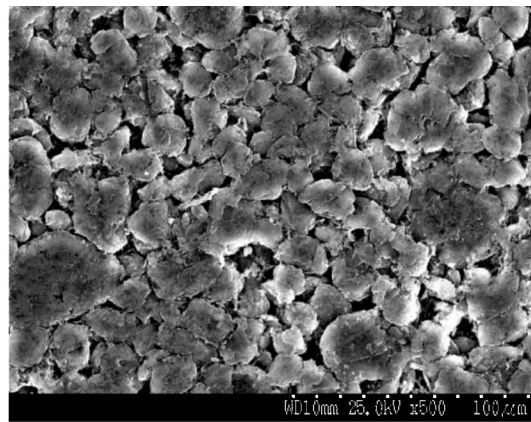
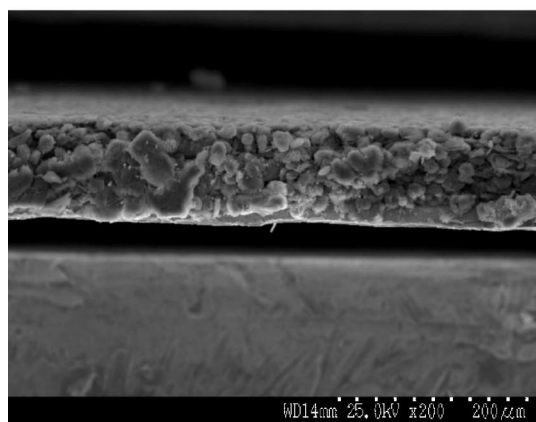


**Figure 9.** Images showing the Li-ion anode particles of SL-20 natural graphite under pressure 300 kg/cm<sup>2</sup>. The image on the left shows the cross-sectional plane; the one on the right shows the horizontal plane.

**Table IV. Experimental determined conductivity and percolation threshold for SL-20, GDR-6, and GDR-14 graphite. Estimated percolation thresholds were determined via linear extrapolation of conductivity measured at pressure 0 and 100 kg/cm<sup>2</sup>.**

Graphite type	Applied pressure (kg/cm <sup>2</sup> )	Matl. thickness (mm)	Volume fraction (%)	Particle length (μm)	Particle diam (μm)	Aspect ratio $\epsilon$	$t/b$	Conductivity ( $\Omega^{-1} \text{cm}^{-1}$ )	Estimated critical volume fraction (%)
SL-20	0	0.154	40.64	23.23	16.64	1.41	9.25	0.66	31.6
	100	0.104	67.35	24.25	16.96	1.44	6.13	2.62	
	200	0.090	82.69	22.63	16.70	1.38	5.39	5.32	
	300	0.084	90.07	22.43	16.07	1.40	5.23	5.24	
GDR-6	0	0.125	44.81	31.47	21.83	1.46	5.73	3.79	24.4
	100	0.10	57.65	30.82	22.20	1.40	4.50	6.17	
	200	0.078	67.73	31.35	23.26	1.36	3.35	15.6	
	300	0.08	80.73	31.22	22.84	1.38	3.50	14.9	
GDR-14	0	0.116	40.46	29.46	20.82	1.43	5.57	25.3	25.7
	100	0.096	59.80	28.46	20.72	1.38	4.63	58.5	
	200	0.092	66.44	27.04	19.69	1.39	4.67	28.6	
	300	0.087	68.75	25.00	17.46	1.46	4.98	35.6	

nonnegligible proportion of large clusters ( $k \geq 10$ ) arises for systems of ellipsoids ( $\epsilon = 10$ ); this has important implications for image analysis, discussed later.

Distributions of mean cluster size vs. locations along the  $z$  direction are shown in Fig. 7, for spheres (top) and ellipsoids ( $\epsilon = 10$ , bottom). One thousand realizations were generated and analyzed for each volume fraction; averaged results are reported. The number of particles in each realization varied from 5000 to 10,000, depending on the volume fraction used. Also, because of the half-plane symmetry, position is normalized by the half-thickness of the layer model, such that "0" represents the lower surface of the domain, and "1" represents the midplane. The mean cluster size is normalized by the value at the midplane.

Figure 7 clearly shows the  $z$  direction bias in cluster distributions for finite, 3D domains. Clusters are smallest near boundaries and increase monotonically to reach a maximum at the midplane. However, this bias is pronounced at "intermediate" (in terms of percolation) volume fractions only. At low volume fractions relative to percolation onset, the lack of particle interaction results in distinct, uncorrelated particles, and few clusters overall. At the other extreme, for volume fractions well above the percolation threshold, particles are highly correlated, and large clusters arise. Thus, mean cluster size becomes invariant with respect to spatial location, due to strong interparticle connections.

Obviously, mean cluster size in a finite particulate system is always bounded; mean cluster size in an infinite system is always unbounded. In finite systems, for volume fractions of an intermediate value relative to percolation onset (e.g., 7% or so for spheres and 30% or so for ellipsoids, per Fig. 7), the boundary imposes a significant constraint on cluster formation. The mean cluster size increases exponentially at the midplane as the system's volume fraction approaches its percolation point. Thus, we find that the variance in mean cluster sizes, through the  $z$  direction, is maximum at the percolation point.

This trend can be even more clearly seen in Fig. 8, in which normalized mean cluster sizes at the boundary are reported as a function of volume fractions for spheres (Fig. 8, top) and ellipsoids (Fig. 8, bottom). For example, normalized cluster size is a minimum at the percolation point of  $f = 0.07$  in Fig. 8 (bottom). Interestingly, the normalized minimum cluster size is around 0.4 for systems of both spheres and ellipsoids. Similar values were also observed for other aspect ratios, and we state that normalized minimum cluster is apparently invariant with respect to particle aspect ratio, for large thicknesses relative to particle size.

The findings reported here have some significance in the image analysis of porous and infused materials. For example, a common question for infused materials is whether particles are spatially uncorrelated, i.e., whether particle locations are truly random. Agglomeration can be desirable or undesirable for a given application; often,

observations of clusters of particles lead immediately to the conclusion that there is a particular physics involved.<sup>58-62</sup> However, our results indicate that even at volume fractions, nonnegligible numbers of large clusters arise for random systems of particles. Thus, Tables II and III could be used to compare cluster statistics for random and real materials, to determine whether or not observed clustering is consistent with random arrangement.

This is perhaps even more significant for what we have termed "finite layers," i.e., domains having thicknesses of approximately five times the particle thickness  $2b$ . Our results show that for volume fractions below the percolation threshold, significant variances arise for mean cluster sizes, and boundary effects produce denser arrangements of particles near the midplane. In materials wherein compression is used to densify thin layers,<sup>63,64</sup> differentiation of the possibly inhomogeneous deformation of these materials from statistical effects in finite layers is important in understanding the percolative consequences of postprocessing.

### Experimental Verification

For verification of our simulations and approximate analytic solutions, we compared measured conductivities<sup>64,65</sup> of three different natural graphite Li-ion anode materials comprised of purified natural graphite from Superior Graphite (SL-20, as shown in Fig. 9), and

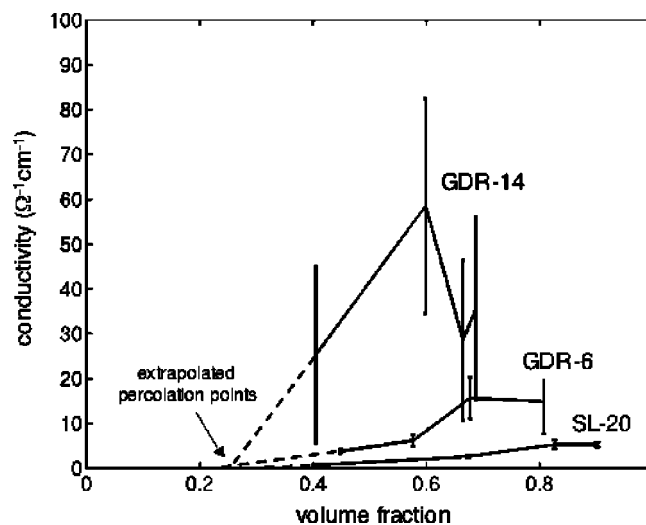


**Figure 10.** Experimental determination of percolation point via linear extrapolation of conductivity against volume fraction. The mean values of conductivity were used in extrapolation, although the standard deviations of the experimental results are also shown in the plot.

**Table V. Estimated percolation threshold for the same materials in Table IV, using linear interpolation of the simulation data listed in Table I. The required parameters were obtained from Table IV.**

Graphite type	Average $\epsilon$	Average $t/b$	$C_1$	$C_2$	$C_3$	$C_4$	$f_c$ (%)	$f_{2D}$ (%)	$f_{3D}$ (%)
SL-20	1.408	6.50	0.2762	1.0013	-0.5054	0.1389	28.2	51.4	27.5
GDR-6	1.400	4.27	0.2765	1.0030	-0.5071	0.1391	29.6	51.4	27.5
GDR-14	1.415	4.96	0.2759	0.9998	-0.5039	0.1388	28.9	51.3	27.4

natural graphite from Mitsui Mining, with 6 (GDR-6) and 14 (GDR-14) weight percentage coatings of amorphous carbons, respectively. Three different anode densities (volume fractions) of each material were thus obtained for each of the three materials. Imaging of all materials was performed as described previously.<sup>64</sup> In previous work, we had compared our conductivity results to only 2D models of conduction, from direct simulations of particle systems, using image analysis data as input.<sup>64</sup>

Our experimental results, along with estimated critical volume fractions, are tabulated in Table IV. The effective conductivity was determined from recorded current and voltage, and the percolation threshold was estimated via linear extrapolation of conductivity against volume fraction. Specifically, we evaluated the mean values of conductivity at different volume fractions and connected the two data points at the smallest volume fractions. We then extended the line to cross the horizontal axis. The volume fraction at which the conductivity is extrapolated to be zero was identified as percolation onset, as shown in Fig. 10. The measured ratio of particle diameter to layer thickness is used as an input parameter in the later simulation. Because thicknesses were altered by application of pressure, the diameter-to-thickness ratios were averaged as needed.

### Conclusions

We studied transitions in cluster properties and percolation points in finite and infinite networks, comprised of equisized, fully penetrable ellipses and ellipsoids. In doing so, we developed numerical results for specific properties and also approximate relations for a wide range of both finite and infinite systems which may prove useful in the design of materials or sensor systems. For the special case wherein the major axes of particles are parallel to the  $x$ - $y$  plane, we showed that percolation thresholds were significantly higher; this may prove important in systems containing preferential orientation of particles. Additionally, boundary conditions affecting clustering formation and the cluster properties were investigated in terms of their effect on nonuniformity in particle clustering in the  $z$  direction.

Excellent agreement between measured percolation thresholds (Table IV) and interpolated simulation results (Table V) were found using the approximate formulas; errors less than 5% were found, in terms of volume fraction. To accurately locate the critical volume fraction, data are needed at smaller volume fraction intervals, and higher order curve fitting techniques may be merited. A significant drawback of our approach was the extrapolation of the percolation point at volume fractions significantly away from the percolation points (see Fig. 10). Improved accuracy of any extrapolation would be expected with additional measurements.

Percolation thresholds in the systems studied are much closer to those of 3D, rather than 2D systems. The average diameter-to-thickness ratio is 6.5 for SL-20 graphite, 4.27 for GDR-6, and 4.96 for GDR-14, all of which are close to 5.0, the apparently universal transition point of percolation from two to three dimensions, lending further support to our approach. A somewhat surprisingly low threshold was found for thicknesses of systems wherein a finite-thickness model, or even a 3D model must be used vs. a 2D model, of around  $t/b = 5$ . This threshold is important for both estimation of percolation point, and cluster properties.

The effect of boundaries on particle clustering was also important. We observed that mean cluster size is minimized at boundaries in the  $z$  direction, reaching a maximum at the midplane. The bound-

ary effect disappears for both low- and high-volume fractions relative to the percolation volume fraction. We also pointed out that cluster statistics should properly be used for interpretation of images of real materials, specifically in drawing conclusions about randomness in packing, and determination of the effects of processing on cluster distribution for low volume fractions relative to the percolation fraction.

In future work, we aim to apply these statistical models to both designs of materials, and of sensor systems, in finite domains.

### Acknowledgments

Support for this work provided by the Defense Advanced Research Projects Agency and the Office of Naval Research through the Synthetic Multifunctional Materials (SMFM) Program (Dr. Leo Christodoulou and Dr. Steve Fishman, Program Monitors), from National Science Foundation Presidential Early Career Award for Scientists and Engineers (A.M.S.), and the W. M. Keck Foundation is gratefully acknowledged.

*The University of Michigan assisted in meeting the publication costs of this article.*

### References

- Z. G. Qi and A. Kaufman, *J. Power Sources*, **113**, 37 (2003).
- E. Quartarone, P. Mustarelli, and A. Magistris, *J. Phys. Chem. B*, **106**, 10828 (2002).
- L. A. L. de Almeida, G. S. Deep, A. M. N. Lima, and H. Neff, *Appl. Phys. Lett.*, **77**, 4365 (2000).
- D. E. Williams and K. F. E. Pratt, *Sens. Actuators B*, **70**, 214 (2000).
- G. Blaser, T. Ruhl, C. Diehl, M. Ulrich, and D. Kohl, *Physica A*, **266**, 218 (1999).
- L. Berhan and A. M. Sastry, *J. Compos. Mater.*, **37**, 715 (2003).
- C. W. Wang, K. A. Cook, and A. M. Sastry, *J. Electrochem. Soc.*, **150**, A385 (2003).
- X. Cheng, A. M. Sastry, and B. E. Layton, *ASME J. Eng. Mater. Technol.*, **123**, 12 (2001).
- O. Pekcan and S. Ugur, *J. Colloid Interface Sci.*, **251**, 409 (2002).
- H. K. Janssen, K. Oerding, F. van Wijland, and H. J. Hilhorst, *Eur. Phys. J. B*, **7**, 137 (1999).
- N. Zekri and J. P. Clerc, *Phys. Rev. E*, **64**, 056115 (2001).
- M. A. Fuentes and M. N. Kuperman, *Physica A*, **267**, 471 (1999).
- G. J. Gibson, *Appl. Statistics-J. Royal Statistical Soc. Series C*, **46**, 215 (1997).
- U. Nigge, H. D. Wiemhofer, E. W. J. Romer, H. J. M. Bouwmeester, and T. R. Schulte, *Solid State Ionics*, **146**, 163 (2002).
- G. Blaser, T. Ruhl, C. Diehl, M. Ulrich, and D. Kohl, *Physica A*, **266**, 218 (1999).
- J. Quintanilla and S. Torquato, *Phys. Rev. E*, **54**, 5331 (1996).
- J. Quintanilla and S. Torquato, *Adv. Appl. Probab.*, **29**, 327 (1997).
- S. W. Haan and R. Zwanzig, *J. Phys. A*, **10**, 1547 (1977).
- Y. B. Yi and A. M. Sastry, *Phys. Rev. E*, **66**, 066130 (2002).
- G. E. Pike and C. H. Seager, *Phys. Rev. B*, **10**, 1421 (1974).
- I. Balberg and N. Binenbaum, *Phys. Rev. B*, **28**, 3799 (1983).
- I. Balberg, N. Binenbaum, and N. Wagner, *Phys. Rev. Lett.*, **52**, 1465 (1984).
- W. Xia and M. F. Thorpe, *Phys. Rev. A*, **38**, 2650 (1988).
- E. J. Garboczi, K. A. Snyder, J. F. Douglas, and M. F. Thorpe, *Phys. Rev. E*, **52**, 819 (1995).
- A. M. Sastry, Sandia Report SAND94-2884 (1994).
- Z. G. Qi and A. Kaufman, *J. Power Sources*, **113**, 37 (2003).
- E. Quartarone, P. Mustarelli, and A. Magistris, *J. Phys. Chem. B*, **106**, 10828 (2002).
- M. Brasuel, R. Kopelman, T. J. Miller, R. Tjalkens, and M. A. Philbert, *Anal. Chem.*, **73**, 2221 (2001).
- H. A. Clark, S. L. R. Barker, M. Brasuel, M. T. Miller, E. Monson, S. Parus, Z. Y. Shi, A. Song, B. Thorsrud, R. Kopelman, A. Ade, W. Meixner, B. Athey, M. Hoyer, D. Hill, R. Lightle, and M. A. Philbert, *Sens. Actuators B*, **51**, 12 (1998).
- H. A. Clark, M. Hoyer, M. A. Philbert, and R. Kopelman, *Anal. Chem.*, **71**, 4831 (1999).
- Y. B. Yi, H. Wang, A. M. Sastry, and L. Lamberson, Paper 4698-23, SPIE Conference, San Diego, CA, March 2002.
- M. D. Penrose, *Adv. Appl. Probab.*, **23**, 536 (1991).

33. A. Coniglio, U. Deangelis, A. Forlani, and G. Lauro, *J. Phys. A*, **10**, 219 (1977).
34. A. Coniglio, U. Deangelis, and A. Forlani, *J. Phys. A*, **10**, 1123 (1977).
35. S. Kirkpatrick, *Rev. Mod. Phys.*, **45**, 574 (1973).
36. D. P. Bentz, E. J. Garboczi, and E. S. Lagergren, *Cem. Concr. Aggreg.*, **20**, 129 (1998).
37. E. J. Garboczi and D. P. Bentz, *Cem. Concr. Res.*, **31**, 1501 (2001).
38. N. V. Dokholyan, S. V. Buldyrev, S. Havlin, P. R. King, Y. Lee, and H. E. Stanley, *Physica A*, **266**, 55 (1999).
39. J. S. Andrade, N. Ito, and Y. Shibusa, *Phys. Rev. B*, **54**, 3910 (1996).
40. A. Gabrielli, R. Cafiero, and G. Caldarelli, *J. Phys. A*, **31**, 7429 (1998).
41. C. Thomsen, *Phys. Rev. E*, **65**, 065104 (2002).
42. C. D. Lorenz and R. M. Ziff, *J. Chem. Phys.*, **114**, 3659 (2001).
43. S. Tsubakihara, *Phys. Rev. E*, **62**, 8811 (2000).
44. N. Provatas, M. Naataja, J. Asikainen, S. Majaniemi, M. Alava, and T. Ala-Nissila, *Colloids Surf., A*, **165**, 209 (2000).
45. M. P. Nightingale, *Physica A*, **83**, 561 (1975).
46. D. Stauffer, *Phys. Lett.*, **54B**, 1 (1979).
47. W. J. Boudville and T. C. McGill, *Phys. Rev. B*, **39**, 369 (1989).
48. Y. B. Yi, H. Wang, A. M. Sastry, and C. M. Lastoskie, *Biophys. J.*, Submitted.
49. C. A. Fierke and R. B. Thompson, *Biometals*, **14**, 205 (2001).
50. J. W. Perram and M. S. Wertheim, *J. Comput. Phys.*, **58**, 409 (1985).
51. J. Viellard-Baron, *J. Chem. Phys.*, **56**, 4729 (1972).
52. J. Quintanilla, *Phys. Rev. E*, **63**, 061108 (2001).
53. Y. B. Yi and A. M. Sastry, *Proc. R. Soc. London, Ser. A*, **460**, 2353 (2004).
54. E. K. Yeh, J. Newman, and C. J. Radke, *Colloids Surf., A*, **156**, 137 (1999).
55. S. W. Song, K. A. Striebel, R. P. Reade, G. A. Roberts, and E. J. Cairns, *J. Electrochem. Soc.*, **150**, A121 (2003).
56. S. A. Roach, *The Theory of Random Clumping*, Methuen, London (1968).
57. A. G. Ogston and D. J. Winzor, *J. Phys. Chem.*, **79**, 2496 (1975).
58. S. Simons, Jr., *Powder Technol.*, **87**, 29 (1996).
59. S. Sigrist, R. Jullien, and J. Lahaye, *Cem. Concr. Compos.*, **23**, 153 (2001).
60. M. Staiger, P. Bowen, J. Ketterer, and J. Bohonek, *J. Dispersion Sci. Technol.*, **23**, 619 (2002).
61. J. Mizsei and V. Lantto, *Phys. Scr., T*, **69**, 233 (1997).
62. K. Sieradzki, K. Bailey, and T. L. Alford, *Appl. Phys. Lett.*, **79**, 3401 (2001).
63. F. Delie and D. Bouvard, *Acta Mater.*, **46**, 3905 (1998).
64. C. W. Wang, Y. B. Yi, A. M. Sastry, K. A. Striebel, and J. Shim, *J. Electrochem. Soc.*, In press.
65. C. W. Wang, K. A. Cook, and A. M. Sastry, *J. Electrochem. Soc.*, **150**, A385 (2003).